Chemical banding revealed by chemical etching in a cold-rolled metastable stainless steel

C. Celada [a,*], I. Toda-Caraballo [b], B. Kim[b], D. San Martín [a]

[a]*MATERALIA Research Group, Department of Physical Metallurgy, Centro Nacional de Investigaciones Metalúrgicas (CENIM – CSIC), Av. Gregorio del Amo 8, 28040 Madrid, Spain.*

[b]*Department of Materials Science and Metallurgy, University of Cambridge, Pembroke Street, Cambridge CB2 3QZ, UK.*

E-mails: c.celada@cenim.csic.es; it247@cam.ac.uk; bnk20@cam.ac.uk; dsm@cenim.csic.es.

* Corresponding author:

Carola A. de Celada

Department of Physical Metallurgy, CENIM-CSIC.

Av. Gregorio del Amo, 8, 28040, Madrid, Spain.

Tel: 0034 91 553 89 00 (Ext 272)

Fax: 0034 91 534 7425

E-mail: c.celada@cenim.csic.es

Materials Characterization 84 (2013) 142-152

http://dx.doi.org/10.1016/j.matchar.2013.07.018

Abstract

The current work describes the metallographic characterization of the initial microstructure of a cold rolled precipitation hardening semi-austenitic stainless steel (12Cr-9Ni-4Mo-2Cu-1Ti, in wt. %). The use of the Lichtenegger and Blöch (L-B) colour etching solution has been shown to reveal not only the phases present in the microstructure, but also the existence of chemical banding along the rolling direction. The L-B reagent has been found to colour the microstructure in bands depending on what alloying elements have segregated to each band. Two-dimensional electron probe microanalysis (EPMA) maps have shown that Ni, Cu and Ti segregate together in the bands, while Cr has an opposite behaviour. Mo has a mixed segregation behaviour although much weaker than the other elements and more prompt to segregate like Ni does. A direct comparison of light optical micrographs with the EPMA maps of the same area of the microstructure has enable to establish a direct relationship between the alloying element band concentration and the resulting etching colour contrast obtained with the L-B reagent. Thermodynamic calculations predict that solidification in this steel takes place with ferrite as the primary phase. Equilibrium partitioning coefficient calculations seem to support the observed segregation patterns.

Keywords

Austenitic stainless steel; segregation; colour etching; chemical banding; EPMA measurements.

1. Introduction

Microstructural banding occurs quite commonly in high-strength high-alloyed steels [1,2]. Its presence has been attributed to the segregation of alloying elements during solidification. In this process, alloying elements are rejected from δ-ferrite dendrites, leading to a high solute content in the interdendritic regions. In subsequent forming operations, such as extrusion or rolling, areas in the microstructure exhibiting segregation align along the material flow direction in the form of bands, resulting in the so-called chemical banding. Band width and pattern vary with the degree of inhomogeneity and the mechanical processing history [3,4]. This inhomogeneous solute distribution might give raise to a microstructural banding during solid-solid phase transformations [5]. In this respect Verhoeven *et al.* [6] have written an extensive review concerning microsegregation induced banding phenomena in steels and have described the characteristics of banding present in different types of steels.

The segregation of alloying elements can produce different etching responses, which can lead to the disclosure of regions of different composition. To the author's knowledge, one of the first to reveal the presence of microsegregation was Stead [6]. His Cu based etchants (Stead's reagents), are extremely effective at revealing the relative phosphorous concentration in steels or phosphorous segregation to eutectoid cells in gray cast iron [6,7]. In the same sense, a large number of etchants that reveal chemical banding/segregation have been reported afterwards [5-8]. It is worthwhile to point out the difference between etchants that indirectly reveal chemical banding, as the bands consist of different phases resulting from a previous microsegregation [5,6]; and etchants which vary the coloration according to the alloying element content in monophasic microstructures [7,8], as has been investigated in this study.

In high alloyed maraging steels it has been shown that the microsegregation of alloying elements can be removed or slightly reduced by annealing for several hours at high austenitization temperature [1]. This heat treatment procedure is also a standard practice in

low alloy steels to reduce the chemical banding observed in, for example, carbon-manganese steels [9]. The temperatures and times needed to chemically homogenize the microstructure depend on the element that appears segregated, the high temperature matrix phase (austenite, martensite, ferrite) and steel composition. Chemically banded structures and their evolution with homogenization treatments have been studied by means of electron probe microanalysis (EPMA) [5,10]. In general, this technique has been proven very useful to investigate the composition of different phases in steels and thus help in the study phase transformations or assess the quality of steel products [11-15].

The maraging stainless steel under study in this work was developed in the mid-nighties as a promising alloy for very demanding applications such as for surgical needles [16]. Although due to the excellent combination of mechanical properties of this type of steels it could be potentially attractive for other applications [17,18]. Since then, several investigations have been published to obtain a deeper physical understanding of its unique properties. In the metastable austenitic annealed state (γ), it transforms to martensite (α') phase either under the application of stresses/strains or when subjected to cryogenic treatments [19]. In addition, it has been shown recently that this transformation ($\gamma \rightarrow \alpha'$) can be accelerated by applying external magnetic fields [20-22]. After its transformation to martensite, the optimum mechanical properties are obtained by precipitation hardening of nano-intermetallic phases [23]. For this investigation, this steel has been received as cold-rolled sheets which contain an almost fully martensitic microstructure. The research described in this manuscript is part of a wider investigation concerning the reaustinization (martensite to austenite transformation) of cold-rolled sheets of this metastable stainless steel and the achievement of sub-micrometer size austenitic microstructures with improved mechanical properties. Using this approach, very interesting mechanical properties have been obtained in similar steels [24, 25]. Chemical banding has been observed in the initial cold-rolled martensitic microstructure of this steel. Previous research has shown that the presence of chemical banding affects phase

transformations and properties of steels [10, 26]. Thus, it should be expected that it will also have a prominent influence on the nucleation and growth of austenite during the reaustinization process. For this reason the phases present in the initial microstructure and the chemical banding observed in the as-received microstructure have been thoroughly characterized by light optical microscopy (LOM), scanning electron microscopy (SEM), EPMA and X-ray diffraction (XRD). Furthermore, an attempt was made to eliminate or minimize this chemical banding by applying high temperature heat treatments. However, it was not the intention of this paper to provide a detail investigation on the influence of high temperature heat treatments on the chemical banding detected in the initial microstructure. Results corresponding to a heat treatment performed at 1100 ^{o}C for 18 hours are described and have been characterized using some of the experimental techniques also used to characterize the as-received microstructure. Higher temperatures have been avoided as the delta ferrite formation has been detected. It should be added that the application of these heat treatments transforms the initial martensitic microstructure to austenite and makes this high temperature phase so unstable that it quickly transforms back to martensite isothermally after cooling down to room temperature [27].

The results of this characterization show that a direct relationship can be established between the chemical banding characterized by EPMA and the etching contrast revealed by chemical etching using Lichtenegger-Blöch (L-B) reagent. The application of this chemical etchant to other martensitic stainless steels could be a fast procedure to reveal the presence of chemical banding.

2. Materials and Methods

Steel samples have been received in the form of cold-rolled sheets with a thickness of 0.45 mm approximately. These sheets have been obtained after a process of continuous casting followed by hot-rolling and cold-rolling until the target thickness (0.45 mm) is obtained. The

application of heavy cold-rolling not only causes the transformation of the as-cast metastable austenite into martensite, but also the severe deformation of the strained induced martensite. As it will be shown later on, a small volume fraction of retained austenite and chi-phase (χ) precipitates (<1 μm) have been found in the microstructure.

Due to its importance for this work, several methods have been used to determine the chemical composition of the considered steel. An accurate quantitative determination of the main alloying elements has been done using different techniques: the Ni content has been obtained by gravimetric analysis, the Cr content by volumetric analysis, and the Mo, Cu, Ti and Al contents have been determined by atomic absorption spectrometry (VARIAN, SpectrAA 220 FS). On the other hand, a semi-quantitative analysis of Si and Mn has been done by using a "Bruker" Wavelength dispersive X-ray fluorescence spectrometer (WDXRF). The chemical composition of the steel determined by quantitative and semi-quantitative techniques is shown in Table 1.

With the aim of studying which phases are present in the initial microstructure as well as potential microsegregation problems, the metallographic characterization has been carried out on the cross section (perpendicular to the rolling direction) of the steel sheets. Steel specimens have been ground and polished using standard metallographic preparation procedures, finishing with 1 μm diamond paste. For XRD and SEM inspection, samples were finalized using a colloidal silica solution. Subsequently, for SEM and LOM observation the microstructure has been etched with three different chemical solutions whose composition is shown in Table 2. The microstructure was inspected using one optical microscope (Nikon Epiphot 200) and two scanning electron microscopes (a FEG-SEM Hitachi S4800 and a FEG-SEM JEOL J8M6500). Phase identification has been performed by using a Siemens D5000 X-ray diffractometer, which operates with Co Kα-radiation. Diffraction patterns have been recorded on the cross section and on the surface along the rolling direction. In order to have a large enough material

surface to inspect the cross section (thickness of 0.45 mm) up to ten samples were mounted together.

The microsegregation of alloying elements (Cr, Ni, Mo, Cu and Ti) has been investigated by means of EPMA. These measurements have been performed using a JEOL JXA 8900R microprobe with a wavelength dispersive spectrometer (WDS) at the ICTS National Centre for Electron Microscopy (CNME), located at the Complutense University of Madrid [28]. The homogenization heat treatments were performed to find out their effectiveness on reducing or eliminating the banded structure. This heat treatment was carried out using the high precision furnace of a high resolution dilatometer (Adamel Lhomargy DT1000). Samples of 12 mm in height and 4 mm in width were heated at 1100 ^{o}C for 18 hours in a vacuum atmosphere of 10^{-1} mbar. Two-dimensional (2D) EPMA maps have been recorded in as-received and heat treated samples using a step size of 1 μm over an area of 450 x 200 μm^2, which gives qualitative information about the local concentrations of the elements analyzed. Steel samples have been prepared for EPMA in the same way as for LOM observation. Optical micrographs were also taken of the areas studied with EPMA for comparison.

3. Results

3.1. X-ray Diffraction

Fig. 1a and 1c show X-ray diffraction patterns undertaken on the surfaces perpendicular to the rolling and to the normal directions of the as-received steel sheets, respectively. Fig. 1b and 1d highlight a specific angle range of Fig. 1a and 1c where positions of specific χ-phase diffraction peaks have been pointed out by arrows. These patterns show that the main phase present in the cold-rolled as-received microstructure is martensite. As it would be expected, the martensite phase shows a very strong preferential texture induced by the severe cold-rolling: (110) in the cross section and (211) in the longitudinal section. There is also a small amount of χ-phase precipitates and retained austenite. The χ-phase is a hard and brittle

intermetallic phase whose basic composition is $Fe_{36}Cr_{12}Mo_{10}$, although it usually contains other elements like Ti or Ni [29-31]. Peaks associated with austenite have only been detected in sample sections perpendicular to the normal direction (Fig. 1c and 1d). This could be explained because that section analysed contained a larger amount of austenite compared to the bulk of the material (Fig. 1b and 1d). Since the peaks corresponding to the austenite have not been detected in Fig. 1a, and because the detection limit of XRD measurements can be regarded as around ~0.02-0.03, it could be concluded that the volume fraction of austenite in this cold-rolled material is below this amount (0.02-0.03). The presence of a strong texture in the material could also make it more difficult to detect the austenite peak in the transversal section.

3.2. Scanning electron and light optical microscopy

Fig. 2 shows a set of secondary electron SEM micrographs and an optical micrograph of the as-received microstructure. Fig. 2a displays the microstructure after electrolytic etching for 10 seconds at 15 V dc with a 10 % oxalic acid solution. This etching method reveals second phases and leaves the martensitic matrix basically unetched. The big, cubic shaped particles are titanium nitride (TiN) precipitates. Titanium has a high affinity for nitrogen, as well as for carbon, and thus it binds the residual nitrogen and/or carbon present in the steel leading to the formation of both, nitrides TiN and carbo-nitrides Ti(CN) [32]. On the other hand, the smaller and brighter particles are χ-phase. As can be observed in Fig. 2a, a number of holes are present in the microstructure because some χ-phase precipitates have been partially consumed/extracted from the matrix. The formation of χ-phase precipitates results in a decrease in the Cr content around them, which gives rise to an extremely localized corrosion in the course of the electrolytic etching. The microstructure that displays Fig. 2b has been etched with L-B etching solution (Table 2). Although most chemicals, when dissolved in water, generate heat and produce an exothermic reaction, ammonium bifluoride absorbs heat, so the

reaction is endothermic. If the distilled water is at room temperature, the solution gets colder, and the ammonium bifluoride will not dissolve. Consequently, one must heat the water before dissolving the ammonium bifluoride. This etchant is generally used at approximately 25 to 30 ^{o}C, rather than at room temperature [33,34]. However, it has been found that when this etching solution is used hot, around 60 – 80 ^{o}C, more features of the microstructure are revealed in this kind of stainless steels [29]. On the other hand, when using ammonium bifluoride ($NH_4F{\cdot}HF$), one should take in account that in contact with water it will decompose to ammonium fluoride (NH_4F) and hydrofluoric acid (HF). The HF content of the resulting solution makes it very corrosive, toxic and hazardous. Therefore, this solution must be handled with care.

After etching with L-B for 10 seconds at 60 ^{o}C (Fig. 2b), χ-phase precipitates are made visible and appear as elongated or rounded white particles (Fig. 2c). Apart from χ-phase precipitates, retained austenite and δ-ferrite stringers, as identified by SEM-EDX, have been highlighted in this latter picture.

The volume fraction of these phases has been estimated by using the point counting method [35], in more than 10 SEM representative micrographs. The results show a volume fraction of around 0.01 both for the δ-ferrite phase and retained austenite, and around 0.02 for the χ-phase. It should be bared in mind that these numbers might be slightly underestimating the real volume fraction as smaller particles below 50-100 nm are not considered in the estimation of the χ-phase. The identification of the phases has been done by SEM-EDX. The recognition of the χ-phase is rather straightforward, since the content of Mo in the overwhelming majority of precipitates is higher than 8 wt. %. The detection of the retained austenite and δ-ferrite phases has been based on the content of Cr and Ni. The following results have been obtained for retained austenite: (11.2 ± 0.7) wt. % of Ni and (11.4 ± 0.4) wt. % of Cr; for δ-ferrite: (6.1 ± 0.8) wt. % of Ni and (13.1 ± 0.5) wt. % of Cr; and for the martensitic matrix: (8.8 ± 0.6) wt. % of Ni and (11.9 ± 0.6) wt. % of Cr.

Fig. 2d displays an optical micrograph where the microstructure has been revealed by electrolytic etching with NaOH (10 %) at 15 V dc for 10 seconds. After etching, δ-ferrite stringers are clearly revealed, appearing as the black-etching phase. The small black spots, that can also be distinguished, are attributed to the χ-phase. As can be observed, TiN is etched in light yellow and the matrix remains unetched.

Fig. 3 shows an optical micrograph of the complete cross section of the as-received material. In this case the sample has been etched with L-B solution at 60 ^{o}C for 30 seconds. As can be observed, χ-phase precipitates and titanium nitrides remain white, while the martensitic matrix is etched in different colours from yellow and light-brown to dark-brown and dark-blue.

3.3. Electron Probe Microanalysis (EPMA)

EPMA maps for Cr, Ni, Mo, Cu and Ti are shown in Fig. 4b-f. They have been recorded over the same area of 450 x 200 μm^2 that shows the optical micrograph in Fig. 3. However, in order to avoid some undesirable edge effects, the maps have been trimmed up to 447 x 173 μm^2 by using the program ImageJ [36]. Each EPMA map contains the concentration of each element by means of an intensity parameter that can be easily processed to represent the content of each element per recorded pixel. This computation is under the assumption the analysed area has the same average composition as the steel (Table 1), which is reasonable because no significant compositional variations have been observed on a surface along the rolling direction.

Fig. 4a represents the optical micrograph shown in Fig. 3 but transformed to brown scale. There is a clear correlation between the brighter bands of the optical image and the bands with higher content of Ni, Cu and Ti, while low concentration of Cr corresponds to darker bands in the optical image. That means that the L-B reagent is sensitive to the segregation of elements like Ni, Cu, Ti or Cr. However from these results it is not possible to disclose which influences most the etching response.

The presence of intermetallic precipitates in the steel may mask compositional variations of the matrix, as these will appear as very large concentration peaks in the maps. The scale of titanium map (Fig. 4c) is performed to display such compositional variation. It has to be borne in mind that, stoichiometrically, the calculated Ti concentration in TiN is much higher (77.37 wt. %) than the average chemical composition of the steel (1.35 wt. %). For this reason, in order to disclose the titanium segregation behaviour, in the EPMA map the maximum threshold value for this element has been set to 2.5 wt. %. TiN precipitates appear thereby as dark-red cubic phases. In the other concentration maps, the presence of a TiN causes the opposite: very low or null concentration values of the corresponding alloying element. Therefore, to highlight the underlying segregation behavior in the Ni, Cr, Mo or Cu maps, the minimum concentration value was raised from zero to a higher value. This value was chosen for each map with the aim of minimizing the masking influence of TiN particles only, but always keeping it certainly below the minimum concentration value associated to the segregation pattern. Choosing this value was easy as zero concentration values related to TiN particles appear clearly differentiated in these maps and distinguishable from the segregation pattern. For this reason TiN particles appear as dark-blue cubic phases in Fig. 4b and 4d-f. Regarding the concentration maps for chromium and molybdenum, the presence of fine particles (<1 μm) of χ-phase ($Fe_{36}Cr_{12}Mo_{10}$) in the microstructure may also influence peak concentration values found in the maps. According to the stoichiometry of χ-phase, the concentration of Mo (27.7 wt. %) and Cr (17.4 wt. %) is expected to be much higher than their average matrix content (4.05 and 12.00 wt. %, respectively). However, and contrary to the TiN precipitates (size ~3-10 μm), the size of χ-phase precipitates is smaller than the interaction volume excited by the beam (spatial resolution 1-2 μm). This means that the microanalysis spot covers at the same time matrix and χ-phase precipitates. Thus, maximum concentration values of Cr and Mo in the maps due to the presence of these precipitates are lower than it could be expected.

The results shown in Fig. 4 demonstrate that there is a clear chemical banding of Cr, Ni, Cu, and Ti along the thickness of the steel sheets. These results also show that Ni, Cu and Ti segregated in a similar fashion, while Cr has an opposite behaviour. Molybdenum shows a weaker segregation pattern than these other elements and slightly similar to Ni, Cu or Ti. Although this is not clearly visible in the maps from Fig. 4, it can be easily concluded from the results shown in Fig. 5. In this figure, compositional variations of Ni, Cu, Mo and Cr are compared with intensity variations observed in the optical micrograph after etching with L-B solution. These line scans represent variations measured along the white dashed line drawn in Fig 4a. In the concentration maps a line scan going through the same path has been considered. All intensity and concentration data points were normalized by dividing each value by the mean value in addition to a reduction of noise by a curve smoothing. The curve smoothing was done by using the five-point moving average, disclosing the underlying trend of the data and leaving out noise or other fine scale structures, such as sharp maximum and minimum. It has been found that Ni, Cu and Mo follow the same trend than the intensity of the optical micrograph, while Cr trend is opposite. Moreover, this latter alloying element shows a less pronounced segregation pattern than the others. For each maximum or minimum of Cr there is a minimum or maximum of Ni, Cu, Mo and LOM intensity, respectively. It is surprising how in good agreement the trends of Ni, Cu (and Mo to a lesser extend) are with respect to the intensities of the optical micrograph.

Several heat treatments were performed with the aim of eliminating or reducing the chemical banding observed in the initial microstructure. The main concerned of these heat treatments was to avoid the formation of δ-ferrite, which has been reported to nucleate at 1175 ºC after short annealing times [27]. Thermodynamic calculations performed with ThermoCalc software [37] have shown that above 1020 ºC δ-ferrite forms under equilibrium conditions in this steel. However, this temperature is too low to expect diffusion of alloying elements to be fast enough to reach the homogenization of the microstructure within reasonable holding times.

The experiments carried out by the authors, but not discussed in this work, showed that δ-ferrite is formed at 1150 ºC before any homogenization of the microstructure takes places, while at 1100 ºC it starts forming after 24 hours. For this reason the annealing time was reduced down to 18 hours. Fig. 6 shows EPMA maps of the main alloying elements for the cross section of a sample, which was heat treated at 1100 ºC for 18 hours. Although the heat treatments were carried out under vacuum conditions (10^{-1} mbar), holding the sample at high temperature for long times has slightly damaged the sample surfaces. Due to this slight modification of the microstructure caused by the heat treatment, the borders of these maps (~60 μm of each side) have been cropped. To avoid the influence of TiN precipitates on disclosing properly the microsegregation, the minimum cut-off values have been set so as to disclose the segregation behaviour of the elements, as it was done in Fig. 4. As expected, the χ-phase precipitates have been dissolved since Mo contents higher than 8 wt. % were not detected (Fig. 7). After 18 hours of heat treatment the chemical banding has been substantially reduced. Locally (~1-10 μm), chemical element distribution has been significantly homogenized and most micro-bands have disappeared; however some big macro-segregation bands (~100-200 μm in width) remain present and are especially evident for the Cr, Ni and Cu maps.

4. Discussion

4.1. Colour etching and Electron Probe Microanalysis.

4.1.1. Revealing segregation by Colour etching

Colour metallographic etchants react with the specimen surface to form what appears as stable films or tints. Contrary to standard chemical acid etchants, where the corrosion products produced during etching are dissolved into the etchant and phase boundaries are generally the only features revealed, the surface is, generally, not physically altered. Common

tint etchants used for steels are aqueous solutions of sodium metabisulfite ($Na_2S_2O_5$) or potassium metabisulfite ($K_2S_2O_5$) and/or sodium thiosulfate ($Na_2S_2O_3{\cdot}5H_2O$). In these solutions metabisulfite ($S_2O_5^{2-}$) and the thiosulfate ($S_2O_3^{2-}$) ions are the active ingredients. In aqueous or acidic solutions, in contrast to a metallic surface, these ions decompose into sulphur dioxide (SO_2), hydrogen sulphide (H_2S), sulphur, and hydrogen. The SO_2 depassivates surfaces, particularly stainless steel surfaces, promoting film formation. The H_2S provides the sulphur ion (S^{2-}) that creates a sulphide film on the steel surface when ions of iron, nickel, or cobalt are present [34,38]. The colours observed by LOM depend on the thickness of the non-metallic film formed as a result of the chemical reaction between the steel specimen and the reagent. These also depend on the etching conditions and crystallographic orientation of the particular phase [39]. Several colour etching solution used in stainless steels have been developed in the last decades; the most popular one is probably Behara and variations to this etchant [8,34,40]; but others like Murakami, L-B or Groesbeck's etching solutions have been found also useful to differentiate phases such as ferrite, austenite, sigma phase or carbides in this type of steels [34]. The L-B colour etching solution has been frequently used in duplex stainless steels to differentiate δ-ferrite from austenite. Some of the authors have used it in the past to differentiate martensite, austenite and the χ-phase in the stainless steel investigated, in annealed condition [29]. In their seminal work [8], Lichtenegger and Blöch studied the usefulness of Behara etching solution and variations to the composition of this etchant. Their results seem to show that increasing the content of potassium metabisulphite and/or changing the hydrochloric acid by ammonium diflouride ($NH_4F{\cdot}HF$) helps revealing chemical banding in austenitic steels. They proposed a reagent, become to be known as L-B etching solution, which was able to differentiate clearly ferrite from austenite and also chemical segregation within austenite in austenitic-ferritic welded materials. Besides, Di Schino *et al.* [4] found that, in low-Ni austenitic stainless steels, the L-B reagent etches yellow the Ni rich austenite and blue the Ni poor austenite. After etching the steel under investigation in this work with the hot L-B

colour etching solution (Fig. 3), it has been clearly observed that the martensitic matrix exhibits a similar etching contrast than the austenite described by Di Schino *et al.* [4]. Martensite is etched in different shades of brown, from yellow and light-brown to dark-brown or dark-blue, and different intensity variations as well. The comparison of the optical micrograph (Fig. 3) with the EPMA maps (Fig. 4) establishes a clear relationship between the content of Ni, Cu, Mo and Ti in solid solution and the colour and brightness resulting after etching. Alloying elements Ni, Cu, Mo and Ti segregate together, whereas the Cr has an opposite behaviour. Bands enriched in Ni are coloured in bright yellow, whereas those depleted in Ni (consequently enriched in Cr) are coloured dark-brown or dark-blue. In any case, it can be concluded that the higher the Ni content the brighter the etching. As the Ni content decreases, the brightness of the etching decreases as well, so that the darkest bands correspond to the lowest Ni contents. This effect is clearly noticeable in the bands of the centre of the sample section.

In addition to the tint etchant, many authors find electrolytic etching the easiest and most effective way of phase identification in stainless steels. The process is rather simple; the specimen becomes the anode and the cathode consists of a non-dissolving material such a stainless steel or pure iron. A simple battery with a direct current is applied at room temperature to activate the etching process. Thus, metal ions are conducted away from the anode into the electrolyte solution, that is, the etching solution. A 10 % aqueous oxalic acid solution is widely used to reveal carbides, second phases and grain structures in austenitic stainless steels. If it is present, this etch will also outline δ-ferrite [38,41], although in our investigation it has been more useful the use of a 10 % solution of NaOH. This later reagent is more commonly used to disclose uniquely the δ-ferrite phase in duplex stainless steels [39]. This electrolytic etchant can also help revealing phases such as the sigma (σ) and χ-phase [42], as it has been show in this work in Fig. 2d.

4.1.2. Effect of homogenization on chemical banding

Fig. 7 shows four charts, in which compositional variations before and after the homogenization treatment are compared for the main alloying elements. Fig. 7 has been performed following the same procedure as for obtaining Fig. 5. As it was discussed previously, the sample exhibits not only a local chemical banding, but also a big macro-segregation of about 150 – 200 nm. Fig. 7 reveals that, after a heat treatment at 1100 ^{o}C for 18 hours, the local chemical banding has been substantially reduced; however, the macro-segregation persists. This macro-segregation is especially noticeable in Ni, Cu and Cr. In the case of Mo, the macro-segregation is less evident. On the other hand, possible maximum peaks related to the χ-phase precipitates have also disappeared, since at 1100 ^{o}C the temperature is high enough to dissolve the χ-phase precipitates completely.

4.2. Solidification mode

It is well known that the presence of chemical banding originates from the solidification process and subsequent processing involved in the manufacturing of the steel. For austenitic stainless steels, the solidification path followed by the melt during cooling has been related in the past to Ni equivalent (Ni_{eq}) and Cr equivalent (Cr_{eq}) of the steel, which are used to simplify a multi-composition system into the Fe-Cr-Ni ternary system [4,15,26]. Depending on the ratio of Ni equivalent an Cr equivalent (Cr_{eq}/Ni_{eq}), the solidification modes of austenitic stainless steels can be divided into the following four types, namely austenitic (A mode), austenitic – ferritic (AF mode), ferritic – austenitic (FA mode) and ferritic solidification (F mode) [15,26]:

A mode: $L \rightarrow L + \gamma \rightarrow \gamma$; $Cr_{eq}/Ni_{eq} < 1.25$;

AF mode: $L \rightarrow L + \gamma \rightarrow L + \delta + \gamma \rightarrow \gamma + \delta \rightarrow \gamma$; $1.25 < Cr_{eq}/Ni_{eq} < 1.48$;

FA mode: $L \rightarrow L + \delta \rightarrow L + \delta + \gamma \rightarrow \gamma + \delta \rightarrow \gamma$; $1.48 < Cr_{eq}/Ni_{eq} < 1.95$;

F mode: $L \rightarrow L + \delta \rightarrow \delta \rightarrow \gamma$; $Cr_{eq}/Ni_{eq} > 1.95$.

Ma *et al.* [26] use the following equations for estimating Ni_{eq} and Cr_{eq}:

$$\mathrm{Ni_{eq}} = (\%\mathrm{Ni}) + 30\,(\%\mathrm{C}) + 30\,(\%\mathrm{N}) + 0.5\,(\%\mathrm{Mn}) \quad (1)$$

$$\mathrm{Cr_{eq}} = (\%\mathrm{Cr}) + (\%\mathrm{Mo}) + 1.5\,(\%\mathrm{Si}) + 0.5\,(\%\mathrm{Nb}) \quad (2)$$

With equations (1) and (2), Cr_{eq} and Ni_{eq} have been calculated for the steel under investigation in this work, resulting 16.75 wt. % and 9.85 wt. %, respectively; and Cr_{eq}/Ni_{eq} as 1.70. So, the solidification mode of the steel falls into FA mode. This solidification mode is divided in two stages: the primary δ-ferrite precipitation stage and the three-phase reaction stage. At the primary δ-ferrite precipitation stage, δ-ferrite dendrites form directly from the melt. As the solidification goes on, it reaches the three-phase reaction stage when eutectic colonies appear among the primary δ-ferrite dendrites [26]. Thermodynamic calculations carried out with ThermoCalc software [37], using TCFE6 (version 6.2) database, predict also that solidification would develop forming first of all δ-ferrite at 1437 ºC and, later on, austenite at 1397 ºC.

Guo *et al.* [15] studied the solidification process in a commercial austenitic stainless steel type 316, which is also a metastable stainless steel. This alloy solidifies under mode FA in a similar way as the stainless steel under investigation in this work. During the solidification of the alloy through δ-ferrite, Guo *et al*. calculated that the equilibrium partitioning coefficients Ni and Cr would be lower and larger than unity, respectively; Ni would tend to partition to the untransformed melt while the amount of Cr would increase in δ-ferrite. This would be expected as it is well known that Cr and Ni stabilize ferrite and austenite phases respectively. In the same sense, the partitioning coefficient of Mo is predicted as lower than unity for the 316 alloy, which would imply that Mo, as for Ni, during the formation of δ-ferrite would partition to the melt and both these elements would appear segregated similarly after solidification at room temperature. Subsequently, if the sample is not quenched, the δ-ferrite would transform to metaestable austenite, but some vermicular δ-ferrite would be likely

retained. Their predictions were in good agreement with the experimental results. Table 3 shows equilibrium partitioning coefficients taken from the work by Guo *et al.* considering δ-ferrite as the primary phase. Similar calculations have been undertaken in this work using ThermoCalc for alloy 316 and also for the alloy investigated in this work (and given in Table 3). For alloy 316, good agreement between both calculations is found for Ni and Cr, but not for Mo. The discrepancy between these calculations is not clear but could be due to the use of different thermodynamic databases.

Equilibrium partitioning coefficient calculations for the alloy investigated in this work (Table 3) predict a strong partitioning of Ni, Cu and Ti to the melt during the formation of δ-ferrite, while Cr and Mo would show an opposite but much weaker behaviour. These predictions would explain the segregation pattern results shown in Fig. 4-5 except for Mo. This element shows a weak segregation behaviour but more similar to Ni, Cu or Ti than for Cr (Fig. 5). The lack of reliable thermodynamic data in this range of molybdenum compositions in novel high alloyed steels could be the origin of the discrepancies found between experiments and calculations. In addition, one should also bear in mind that experimental results are generally far from thermodynamic equilibrium conditions. Despite of the discrepancies and limitations of these calculations, they agree reasonable well with the experimental observations.

Finally, some δ-ferrite has been observed retained at room temperature in this alloy (Fig. 2), feature that has been observed also in the scientific literature for similar alloys like 316 [26]. All these observations would corroborate that, as for alloy 316 used in this discussion for comparison, solidification would take place in this steel through de FA mode.

5. Conclusions

1. The initial microstructure of a cold rolled precipitation hardening semi-austenitic stainless steel has been characterized in this work. The metallographic characterization has been carried out by using different chemical and electrolytic etching solutions. The use of the Lichtenegger

and Blöch (L-B) colour etching solution has been shown to reveal not only the phases present in the microstructure, but also the existence of chemical banding along the rolling direction. The L-B reagent has been found to colour the microstructure in bands depending on what alloying elements have been segregated to each band.

2. Two-dimensional electron probe microanalysis (EPMA) maps have shown that Ni, Cu and Ti segregate together in the bands, while Cr has an opposite behaviour. Mo has a mixed segregation behaviour but more prompt to segregate like Ni does. On the other hand, EPMA has also revealed that, in addition to the local micro-chemical banding (lateral spacing of 1-10 μm), there is also a macro-segregation (100-200 μm).

3. A comparison of the light optical micrographs with the EPMA maps has enable to establish a direct relationship between the alloying element band concentration, especially Ni content, and the resulting etching colour contrast obtained with the L-B reagent.

4. Homogenization heat treatment at 1100 ^{o}C for 18 h has substantially reduced the banded structure. However, this treatment does not seem to affect much the macro-segregation.

5. Thermodynamic calculations predict that solidification in this steel takes place with ferrite as the primary phase (Ferritic-Austenitic mode). Equilibrium partitioning coefficient calculations seem to support the observed segregation patterns.

6. Acknowledgements

Authors are grateful to Centro Nacional de Microscopía Electrónica (CNME), located at Complutense University of Madrid, for the provision of laboratory facilities and to Alfredo Fernández Larios for the technical support. C. Celada and D. San Martín would like to acknowledge the financial support from the Ministerio de Economía y Competitividad (project No. MAT2010-19522). C. Celada is also very grateful to the Consejo Superior de Investigaciones Científicas (CSIC) in the form of a JAE-predoc grant under the program “Junta para la

Ampliación de Estudios", co-funded by the European Social Fund. Dr. Niels H. van Dijk from TUDelft (The Netherlands) is gratefully acknowledged for fruitful discussions.

7. References

[1] Ahmed M, Salam I, Hashmi FH, Khan AQ. Influence of banded structure on the mechanical properties of a high-strength maraging steel. JMEPEG 1997; 6:165-171.

[2] Salmon Cox PH, Reisdorf BG, Pellissier GE. The origin and significance of banding in 18Ni (250) Maraging Steel. Trans AIME 1967; 239:1809-1817.

[3] Scheller PR, Flesch R, and Bleck W. Solidification Morphology and Microstructure Properties at Increased Cooling Rates for 18-8 Cr-Ni Stainless Steel. Adv Eng Mater 1999; 1:209-214.

[4] Di Schino A, Mecozzi MG, Barteri M, Kenny JM. Solidification mode and residual ferrite in low-Ni austenitic stainless steels. J Mater Sci 2000; 35:375-380.

[5] Offerman SE, van Dijk NH, Rekveldt MTh, Sietsma J, van der Zwaag S. Ferrite/pearlite band formation in hot rolled médium carbon steel. Mater Sci Tech 2002; 18: 297-303.

[6] Verhoeven JD. A review of microsegregation induced banding phenomena in steels. J Mater Eng Perform 2000; 9: 286-296.

[7] Radzikowska JM. Effect of specimen preparation on evaluation of cast iron microstructures. Mater Charact 2005; 54:287-304.

[8] Lichtenegger P, Blöch R. Colour Etching of High Alloy Steels. Pract Metallogr 1975; 12: 567-73.

[9] Xu W, Rivera-diaz-del-Castillo PEJ, van der Zwaag S. Ferrite/Pearlite Band Prevention in Dual Phase and TRIP steels: model development. ISIJ Inter 2005;45:380-387.

[10] Stauffer AC, Koss DA, and McKirgan JB. Microstructural Banding and Failure of a Stainless Steel. Metal Mater Trans A 2004;35:1317-1324.

[11] Santofimia MJ, Kwakernaak C, Sloof WG, Zhao L, Sietsma J. Experimental study of the distribution of alloying elements after the formation of epitaxial ferrite upon cooling in a low-carbon steel. Mater Charact 2010; 61:937-942.

[12] Potgieter JH, Cortie MB. Determination of the Microstructure and Alloy Element Distribution in Experimental Duplex Stainless Steels. Mater Charact 1991; 26:155-165.

[13] Perricone MJ, Dupont JN, Anderson TD, Robino CV, Michael JR. An Investigation of the Massive Transformation from Ferrite to Austenite in Laser-Welded Mo-Bearing Stainless Steels. Metall Mater Trans A 2011; 42A:700-716.

[14] Ray A, Dhua SK, Jha S. Electron-Probe Microanalysis: Some Applications in the Assessment of Steel Product Quality. X-Ray Spectrom 1999; 28:41-50.

[15] Guo JQ, Tsukamoto S, Kimura T, Nakae H. Nucleation Process Control of Undercooled Stainless Steel by External Nucleation Seed. Acta Mater 1999; 47:3767-3778.

[16] Liu P, Stigenberg AH, Nilsson J-O. Isothermally Formed Quasicrystalline Precipitates Used For Strengthening in a New Maraging Stainless Steel. Scripta Metall Mater 1994;31:249-254.

[17] Liu P. Relationships between Microstructure and Properties of Stainless Steels—A Few Working Examples. Mater Char 2000; 44:413-424.

[18] Eskandari M, Najafizadeh A, Kermanpur A, and Karimi M. Potential application of nanocrystalline 301 austenitic stainless steel in lightweight vehicle structures. Mater Design 2009; 30:3869-3872.

[19] Post J, Nolles H, Datta K, Geijselaers HJM. Experimental determination of the constitutive behaviour of a metastable austenitic stainless steel. Mater Sci Eng A 2008; 498: 179-190.

[20] San Martin D, van Dijk NH, Jimenez-Melero E, Kampert E, Zeitler U, van der Zwaag S. Real-time martensitic transformation kinetics in maraging steel under high magnetic fields. Mater Sci Eng A 2010; 527: 5241-5245.

[21] San Martin D, Aarts KWP, Rivera-Díaz-del-Castillo PEJ, van Dijk NH, Brück E, van der Zwaag S. Isothermal martensitic transformation in a 12Cr-9Ni-4Mo-2Cu stainless steel in applied magnetic fields. J Magn Magn Mater 2008; 320: 1722-1728.

[22] San Martin D, Jiménez-Melero E, Duffy JA, Honkimäki V, van der Zwaag S, van Dijk NH. Real-time synchrotron X-ray diffraction study on the isothermal martensite transformation of maraging steel in high magnetic fields. J Appl Cryst 2012; 45:748-757.

[23] Hättestrand M, Nilsson J-O, Stiller K, Liu P, and Andersson M. Precipitation hardening in a 12%Cr-9%Ni-4%Mo-2%Cu stainless steel. Acta Mater 2004; 52: 1023-1037.

[24] Moallemi M, Najafizadeh A, Kermanpur A, Rezaee A. Effect of reversion annealing on the formation of nano/ultrafine grained structure in 201 austenitic stainless steel. Mater Sci Eng A 2011;530:378–381.

[25] Kumar BR, Sharma S, Mahato B. Formation of ultrafine grained microstructure in the austenitic stainless steel and its impact on tensile properties. Mater Sci Eng A 2011;528:2209–2216.

[26] Ma JC, Yang YS, Tong WH, Fang Y, Yu Y, Hu ZQ. Microstructural evolution in AISI 304 stainless steel during directional solidification and subsequent solid-state transformation. Mater Sci Eng A 2007;444:64–68.

[27] San Martín D, García-Mateo C. Promoting Isothermal Martensite Formation by High Temperature Heat Treatments in a Precipitation Hardening Austenitic Stainless Steel. Solid State Phenom 2011;172-174:166-171.

[28] http://www.cnme.es/

[29] San Martin D, Rivera Diaz del Castillo PEJ, Peekstok E, van der Zwaag S. A new etching route for revealing the austenite grain boundaries in an 11.4% Cr precipitation hardening semi-austenitic stainless steel. Mater Charact 2007; 58: 455-460.

[30] Xu W, San Martin D, Rivera Díaz del Castillo PEJ, van der Zwaag S. Modelling and characterization of chi-phase grain boundary precipitation during aging of Fe-Cr-Ni-Mo stainless steel. Mater Sci Eng A 2007; 467: 24-32.

[31] Kasper JS. The ordering of atoms in the chi-phase of the iron-chromium-molybdenum system. Acta Metall 1954; 2:456-461.

[32] Folkhard E, Rabensteiner E. Welding Metallurgy of Stainless Steel. New York: Springer-Verlag; 1988.

[33] Bastien PG. The mechanism of formation of banded structures. J Iron Steel Inst 1957; 187: 281-91.

[34] Vander Voort GF. Color Metallography. Metallography and Microstructures. ASM Handbook, Volume 9. 2004: 493-512.

[35] Standard Test Method for Determining Volume Fraction by Systematic Manual Point Count, ASTM E562 – 11 (2011).

[36] ImageJ: Image Processing and Analysis in Java (http://rsb.info.nih.gov/ij/).

[37] ThermoCalc Software AB, KTH (Royal Institute of Technology), Stockholm, Sweden.

[38] Bramfitt BL, Benscoter AO. Metallographer's Guide**:** Practices and Procedures for Irons and Steels. Metals Park, OH, ASM International; 2002, p. 234-239.

[39] Van der Voort GF. Metallography and Microstructures. ASM International, McGraw-Hill Inc.; 2004.

[40] Behara E. Metallographic Reagents Based on Sulfide Films. Praktische Metallographie 1970; 7:242-248.

[41] Van der Voort GF. Metallography: principles and practice. ASM International, McGraw-Hill Inc.; 1994.

[42] Michalska J, Sozanska M. Qualitative and quantitative analysis of σ and χ phases in 2205 duplex stainless steel. Mater Charact 2006; 56: 355-362.

Figure captions

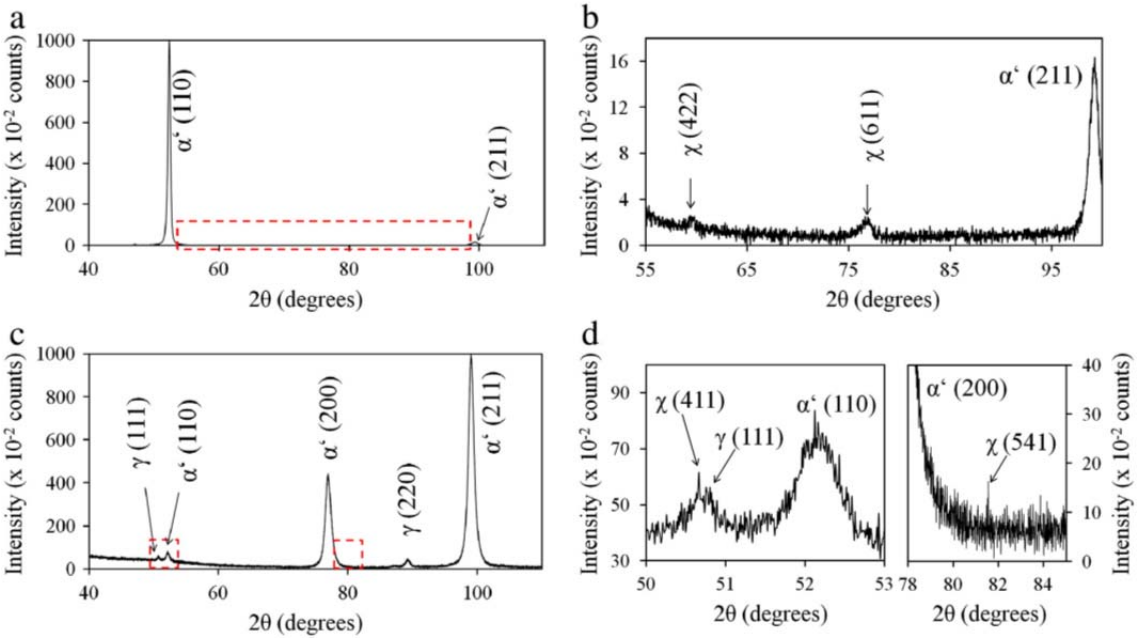

Fig. 1- X-Ray diffraction patterns along the: (a)-(b) Cross section of the sheets; (c)-(d) longitudinal-rolling section. The indices α', γ, and χ stand for martensite, austenite and chi-phase, respectively.

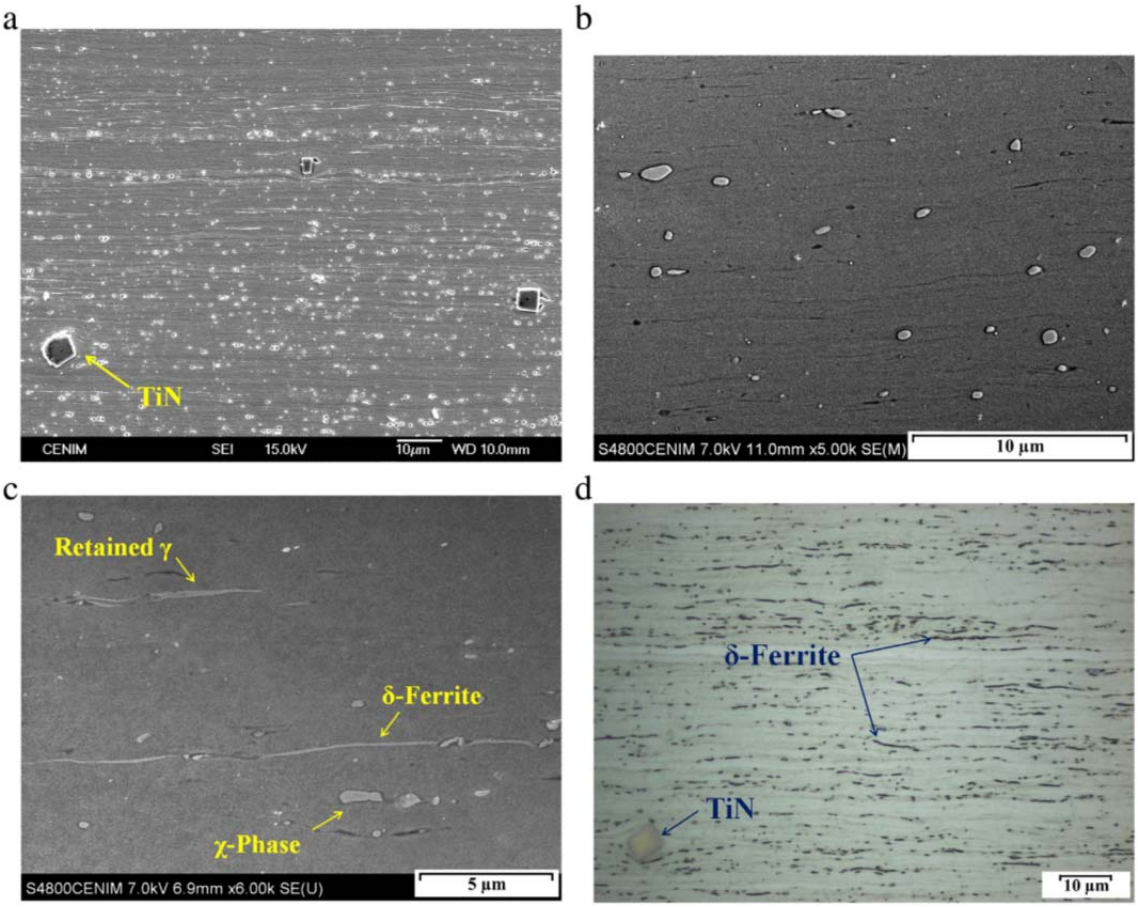

Fig. 2- Secondary electron SEM micrographs of the as-received material after etching with different etchants: (a) electrolytic etching at 15 V for 6 s with an oxalic acid solution (10 %); (b)-(c) etching with hot Lichtenegger-Blöch at 60 ºC for 10 s; and (d) electrolytic etching at 15 V for 10 s with a NaOH (10 %) aqueous solution.

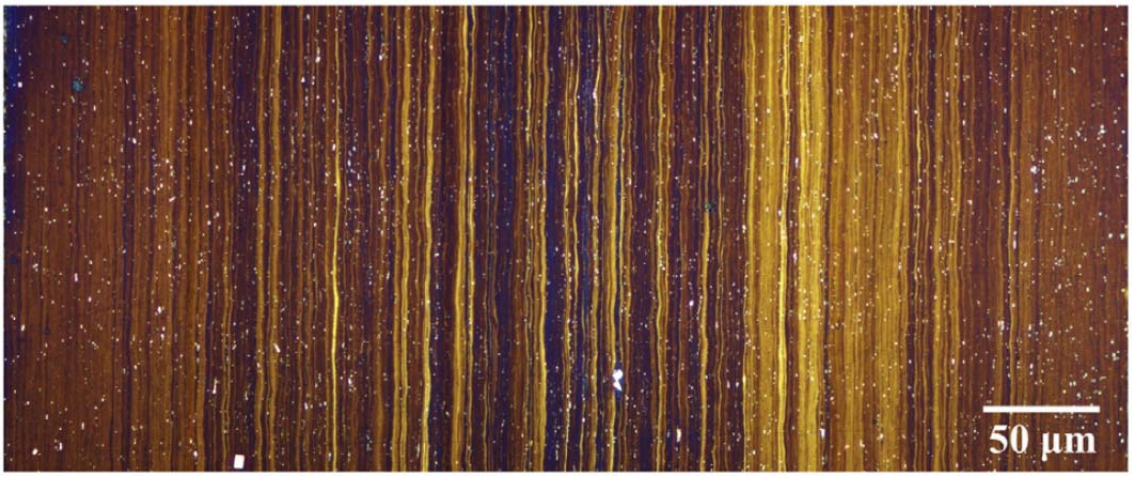

Fig. 3- Optical micrograph of the whole cross section of the as-received microstructure. The sample was etched by using the Lichtenegger-Blöch colour etching solution at 60 ºC for 30 s.

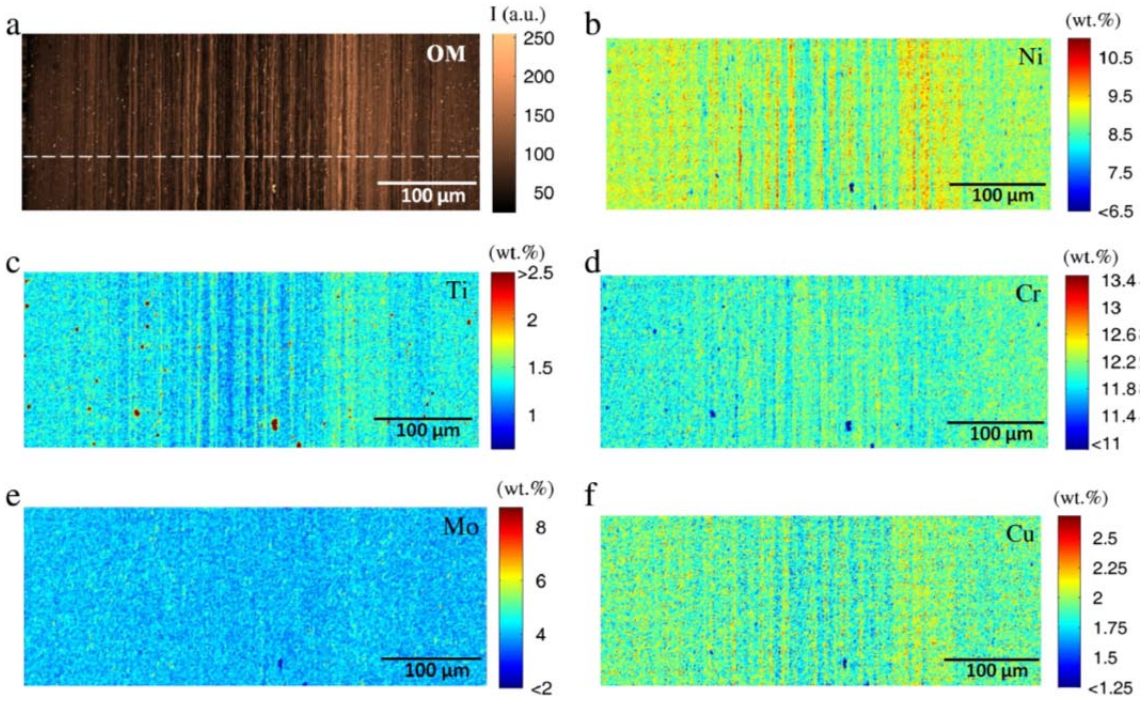

Fig. 4- (a) Optical micrograph transformed to brown scale of the same area where EPMA maps were done; (b)-(f) EPMA maps of the cross section of the as-received material. The scans give qualitative and quantitative information about the local concentration of alloying elements.

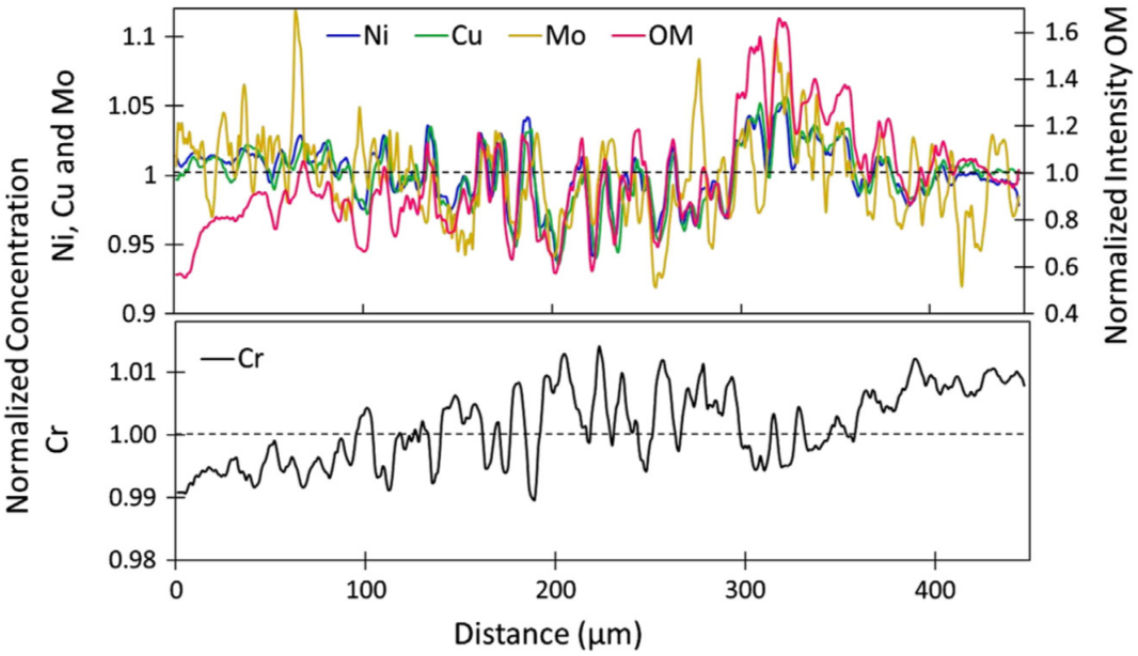

Fig. 5- Line scans obtained from 2D EPMA maps related to Ni, Cu, Mo, Cr and the optical micrograph. The concentration is normalized with the mean concentration (intensity in the case of the optical micrograph) calculated for each element.

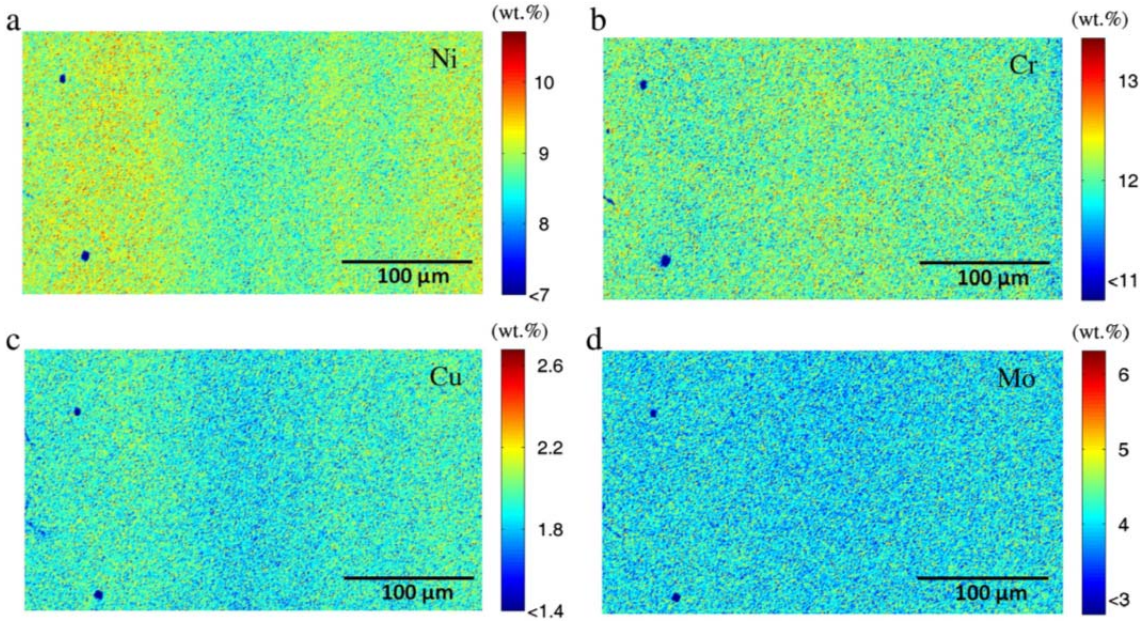

Fig. 6- EPMA maps over an area of 350 x 200 μm^2 of the cross section of a sample that was heat-treated at 1100 ^oC for 18 h.

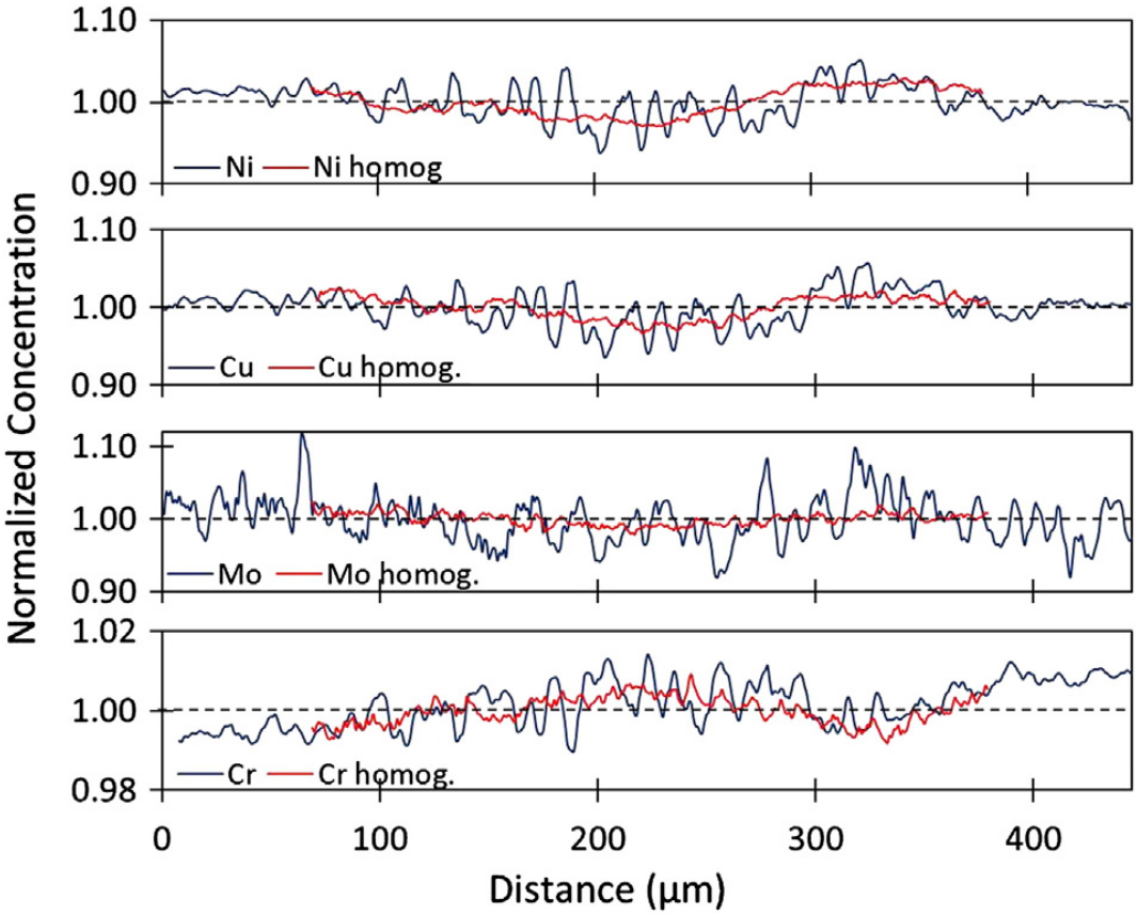

Fig. 7- Comparison between line scans related to the alloying elements Ni, Cu, Cr and Mo for either conditions: in the initial state (blue line) and after homogenization (red line).

Tables

Table 1- Chemical composition of the studied stainless steel (wt. %) with balance Fe.

Cr	Ni	Mo	Cu	Ti	Al	Si	Mn
12±0.09	8.87±0.05	4.05±0.02	1.91±0.01	1.35±0.02	0.39±0.01	0.36±0.04	0.33±0.03

Table 2- Etching solutions employed to disclose the as-received microstructure.

Method	Name	Composition	Conditions
Electrolytic	Oxalic acid	10 g oxalic acid + 100 mL distilled water	Etching at room temperature and 15 V dc for 6 s
Electrolytic	Sodium hydroxide	10 g NaOH + 100 mL distilled water	Etching at room temperature and 15 V dc for 10 s
Standard chemical etching by immersion	Lichtenegger-Blöch (L-B)	20 g $NH_4F{\cdot}HF$ (ammonium difluoride) + 0.5 g $K_2S_2O_5$ (potassium metabisulfite) + 100 mL of distilled water	Etching at 60 ^oC for times between 10 and 30 s

Table 3- Equilibrium partitioning coefficients for Cr, Ni, Mo, Cu and Ti during the initial stages of δ-ferrite formation in alloy 316 and for the alloy under investigation in this work.

Alloy	Cr	Ni	Mo	Cu	Ti
316 [36]	1.02	0.78	0.97		
316 (this work)	1.03	0.76	1.09		
This steel	1.04	0.73	1.06	0.56	0.33